Bending and Buckling Analysis of Functionally Graded Plates using a New Shear Strain Function with Reduced Unknowns

Ali Meftah[*]
University Center of Nour Bachir, Institute of Sciences,
Department of Technology, El Bayadh, 32000, ALGERIA
[*]*genietech2013@yahoo.fr*

ABSTRACT

In this article, functionally graded plates' buckling and bending analyses are investigated using a new shape function. The parabolic transverse shear stresses throughout the thickness are regarded by this function as meeting the shear stress-free surface conditions and enabling an accurate distribution of shear deformation according to the thickness of the plate without integrating shear correction factors. Compared to previous shear theories, this higher-order shear theory has the fewest unknowns. The equations for the functionally graded plates are produced by employing the Hamiltonian principle, and the solutions are obtained using Napier's technique. The outcomes of the current analysis are provided and contrasted with those found in the literature.

Keywords: *Hamilton's Principle; Shape Function; Buckling; Bending*

Introduction

Advanced composite material known as Functionally Graded Material (FGM) has compositions that change depending on the performance needed. The volume fractions of the elements are continuously graded and altered to create the FGM [1], which may be used for a variety of applications including thermal coatings for ceramic engines, gas turbines, nuclear fusion, optical thin layers, biomaterial electronics, and more.

The use of Functionally Graded (FG) plate designs in engineering over the past few years has led to the creation of numerous plate theories that

ISSN 1823-5514, eISSN 2550-164X
Received for review: 2022-10-04
Accepted for publication: 2023-04-17
Published: 2023-09-15
© 2023 College of Engineering,
Universiti Teknologi MARA (UiTM), Malaysia.
https://doi.org/10.24191/jmeche.v20i3.23903

can accurately forecast the vibration, bending, and buckling, behaviours of FG plates [2]. The Classical Plate Theory (CPT) is supported by the concepts of Love Kirchhoff [3]. In which the effects of deformation in transverse shears are ignored and a line parallel to the mean plane of the plate remains perpendicular after deformation. To account for the transverse shear effect, the first-order transverse shear strain theory expands the traditional plate theory. In this case, the tangential stresses remain constant across the thickness of the plate, necessitating the employment of correction factors [4]. There are studies on First-Order Shear Deformation Theory (FSDT) that led to the Reissner - Mindlin plate model, as well as [5]-[9].

Higher Order Shear Deformation Theory (HSDT), a subclass of finer theories, is based on the growth of thickness displacement to an order of two or more. These theories are particularly well adapted to simulate the behaviour of thin, moderately thick, and thick plates, where transverse strain is important. While the higher-order theory is predicated on a nonlinear distribution of the fields in the thickness, the bulk of these models use a Taylor series expansion [10]. The consequences of transverse shear strain and/or transverse normal strain are therefore considered. For these models, correction adjustments are not necessary. These models are mentioned in [7], [11]-[13].

There has been extensive research on the behaviour of functionally graded plates and shells. Cheng and Batra [14] examined the deflections of a homogeneous Kirchhoff plate to those of a simply supported reinforced composite polygonal plate using calculations from first-order shear strain theory and third-shear deformation theory. Cheshmeh et al. [15] employed HSDT to carry out a numerical study on the thermal vibration and buckling analysis of CNTRC-composite plates in various forms. Kulkarni et al. [16] provided an analytical solution based on the inverse trigonometric shear deformation theory for the buckling and bending analysis of FGP. Rectangular FG plates exposed to non-linearly distributed plane edge stresses were examined for buckling [17]. They used a non-mesh technique for their analysis. Additionally, they arrived at a closed-form solution for a simply supported plate by investigating the buckling analysis of a rectangular FG plate utilizing FSDT [18].

The bending analysis of FG plates was provided by [19] using a two-variable improved plate theory. Bodaghi and Saidi [20] focused on the study of buckling caused by different mechanical and thermal loads on rectangular thick FG plates. The third-order shear deformation plate theory was used [21] to develop a new, better plaque theory for FGM plaques that only had four unknown functions. Becheri et al. [22] investigated the buckling and vibration of symmetrically laminated plates. They applied shear deformation theories of the first and third orders for the thermos-elastic deformation of simply supported, functionally graded plates with constrained dimensions, Pelletier and Vel [23] presented an accurate 3-D solution. For the bending

analysis of rectangular FG plates, Zenkour [24] displayed a 3-D elasticity solution, where Young's modulus of the plate is presumptively assumed to vary exponentially with thickness coordinate and Poisson's ratio constant.

The buckling and bending of FG plates are discussed in this article using a novel shape function that is used to develop an HSDT with only four unknowns. The defining differential equations are then reduced to a set of ordinary differential equations linked in the thickness direction and resolved using Navier's methods for simply supported rectangular plates. Numerical findings for the FG plate are shown. To make the results believable, displacements and stresses for different homogenization procedures and exponents in the power law that govern the variation across the thickness of the plate are supplied.

Some Shape Functions

A novel shape function for shear deformation is created and shown using several models, which are listed in Table 1.

Table 1: The shape functions of several HSDT

Models	Shear strain shape function $f(z)$	Derivative $f'(z)$
Reissner et al. [5]	$\frac{5}{2}z\left(1-\frac{4z^2}{3h^2}\right)$	$\frac{5}{2}-\frac{10z^2}{h^2}$
Ambartsumyan [25]	$\frac{z}{2}\left(\frac{h^2}{4}-\frac{z^2}{3}\right)$	$\frac{h^2}{8}-\frac{z^2}{2}$
Soldatos [26]	$hsinh\left(\frac{z}{h}\right)-zcosh\left(\frac{1}{2}\right)$	$cosh\left(\frac{z}{h}\right)-cosh\left(\frac{1}{2}\right)$
Touratier [27] Zenkour [24]	$\frac{h}{\pi}sin\left(\frac{z\pi}{h}\right)$	$cos\left(\frac{z\pi}{h}\right)$
Karama et al. [28]	$ze^{-2\left(\frac{z}{h}\right)^2}$	$e^{-2\left(\frac{z}{h}\right)^2}-\frac{4e^{\frac{-2z^2}{h^2}}z^2}{h^2}$
Grover et al. [29] Benbakhti et al. [30] Meftah et al. [31]	$sinh^{-1}\left(\frac{3z}{h}\right)-z\frac{6}{h\sqrt{13}}$	$\frac{3}{h\sqrt{\frac{9z^2}{h^2}+1}}-\frac{6\sqrt{13}}{13h}$
Present model	$2^5h\left(\frac{z}{2^5h}-\frac{1}{3}\left(\frac{z}{2h}\right)^3\right)$	$1-\left(\frac{2z}{h}\right)^2$

Theoretical Formulations

Take into account an FG plate with the dimensions of *a*, *b*, and *h* as illustrated in Figure 1. The material characteristics of the FG plate vary with plate thickness due to a power law of the elements' volume fractions. The FG plate is made up of ceramic and metal parts.

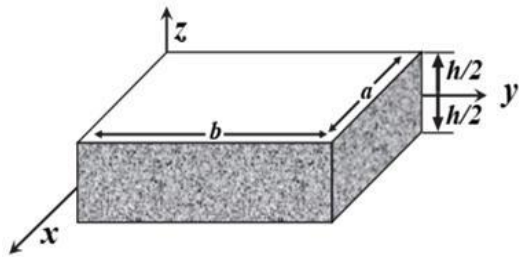

Figure 1: FG plate and coordinates

Properties of efficient materials of FG plates

Thai and Choi [32] denote the material qualities of FG plates.

$$p(z) = (p_c - p_m)v_c + p_m \tag{1}$$

P_c and P_m are the matching material qualities of the ceramic and metal placed on the plate's top and bottom surfaces, respectively. The volume proportion of the ceramic *Vc* material is as follows:

$$V_c(z) = \left(\frac{z}{h} + \frac{1}{2}\right)^p \tag{2}$$

Here p denotes the positive power-law index and $\boldsymbol{z} \in \left[-\frac{\boldsymbol{h}}{\boldsymbol{2}}, \frac{\boldsymbol{h}}{\boldsymbol{2}}\right]$; zirconia distribution along plate thickness, Elastic modulus of the FG plate is provided by the exponential law [24]:

$$E(z) = E_0 e^{p\left(\frac{z}{h} + \frac{1}{2}\right)} \tag{3}$$

The homogenous Elastic modulus of materials is indicated by E_0.

Higher-order shear deformation theories

At the plate's coordinates (*x*, *y*, and *z*), a material point has the following displacement field:

$$u(x,y,z) = u_0(x,y) - z\frac{\partial w_0}{\partial x} - f(z)\frac{\partial \varphi}{\partial x}$$
$$v(x,y,z) = v_0(x,y) - z\frac{\partial w_0}{\partial y} - f(z)\frac{\partial \varphi}{\partial y} \quad (4)$$
$$w(x,y,z) = w_0(x,y)$$

With, *u*, *v*, and *w* the directions are moved in *x*, *y*, *z*, and u_0, v_0, and w_0 are deviations from the median plane, φ owing to bending, the plane rotates. *f(z)* represents the mode shapes determining the thickness-dependent stress and transverse deformation distributions, in this case, I created a new shape function in the form:

$$f(z) = 2^5 h\left[\frac{z}{2^5 h} - \frac{1}{3}\left(\frac{z}{2h}\right)^3\right], \text{and } g(z) = -\frac{df}{dz} \quad (5)$$

Kinematic and constitutive relations

$$\begin{Bmatrix}\varepsilon_{xx}\\ \varepsilon_{yy}\\ \gamma_{xy}\end{Bmatrix} = \begin{Bmatrix}\varepsilon^0_{xx}\\ \varepsilon^0_{yy}\\ \gamma^0_{xy}\end{Bmatrix} + z\begin{Bmatrix}k^b_x\\ k^b_y\\ k^b_{xy}\end{Bmatrix} + f(z)\begin{Bmatrix}k^s_x\\ k^s_y\\ k^s_{xy}\end{Bmatrix}, \begin{Bmatrix}\gamma_{xz}\\ \gamma_{yz}\end{Bmatrix} = g(z)\begin{Bmatrix}\gamma^0_{xz}\\ \gamma^0_{yz}\end{Bmatrix} \quad (6a)$$

$$\begin{Bmatrix}\varepsilon^0_{xx}\\ \varepsilon^0_{yy}\\ \gamma^0_{xy}\end{Bmatrix} = \begin{Bmatrix}\frac{\partial u_0}{\partial x}\\ \frac{\partial v_0}{\partial y}\\ \frac{\partial u_0}{\partial y} + \frac{\partial v_0}{\partial x}\end{Bmatrix}, \begin{Bmatrix}k^b_x\\ k^b_y\\ k^b_{xy}\end{Bmatrix} = \begin{Bmatrix}-\frac{\partial w_0}{\partial x}\\ -\frac{\partial w_0}{\partial y}\\ -2\frac{\partial w_0}{\partial y \partial x}\end{Bmatrix}, \begin{Bmatrix}k^s_x\\ k^s_y\\ k^s_{xy}\end{Bmatrix} = \begin{Bmatrix}-\frac{\partial \varphi_0}{\partial x}\\ -\frac{\partial \varphi_0}{\partial y}\\ -2\frac{\partial \varphi_0}{\partial y \partial x}\end{Bmatrix}, \begin{Bmatrix}\gamma^0_{xz}\\ \gamma^0_{yz}\end{Bmatrix} = \begin{Bmatrix}\frac{\partial \varphi}{\partial x}\\ \frac{\partial \varphi}{\partial y}\end{Bmatrix} \quad (6b)$$

For elastic FGMs, the constitutive relations can be written as follows:

$$\begin{Bmatrix}\sigma_{xx}\\ \sigma_{yy}\\ \tau_{yz}\\ \tau_{xz}\\ \tau_{xy}\end{Bmatrix} = \begin{bmatrix}C_{11} & C_{12} & 0 & 0 & 0\\ C_{12} & C_{22} & 0 & 0 & 0\\ 0 & 0 & C_{44} & 0 & 0\\ 0 & 0 & 0 & C_{55} & 0\\ 0 & 0 & 0 & 0 & C_{66}\end{bmatrix}\begin{Bmatrix}\varepsilon_{xx}\\ \varepsilon_{yy}\\ \gamma_{yz}\\ \gamma_{xz}\\ \gamma_{xy}\end{Bmatrix} \quad (7)$$

where:

$$C_{11}(z) = C_{22}(z) = \frac{E(z)}{1-(\nu(z))^2}, C_{12}(z) = \nu(z)C_{11}(z) \quad (8a)$$

$$C_{44}(z) = C_{55}(z) = C_{66}(z) = \frac{E(z)}{2(1+\nu(z))} \tag{8b}$$

Equations of motion

Here, the constitutive equations and the relevant motion equations for the displacement field are acquired using Hamilton's rule. The analytical formulation of the principle is as follows:

$$\int_0^t \quad (\delta U + \delta V - \delta K)dt = 0 \tag{9}$$

$\boldsymbol{\delta U}$: variation of the deformation energy; $\boldsymbol{\delta V_e}$: work done; $\boldsymbol{\delta K}$: variation of the kinetic energy of the FGM plate. The fluctuation of the plate's strain energy is determined by:

$$\begin{aligned}\delta U = \int_A \int_{-\frac{h}{2}}^{+\frac{h}{2}} & (\sigma_{xx}\delta\varepsilon_{xx} + \sigma_{yy}\delta\varepsilon_{yy} + \tau_{xy}\delta\gamma_{xy} + \tau_{xz}\delta\gamma_{xz} \\ & + \tau_{yz}\delta\gamma_{yz})dAdz \\ = \int_A & [N_{xx}\frac{\partial\delta u_0}{\partial x} - M^b_{xx}\frac{\partial^2\delta w_0}{\partial x^2} - M^s_{xx}\frac{\partial^2\delta\varphi}{\partial x^2} + N_{yy}\frac{\partial\delta v_0}{\partial y} \\ & -M^b_{yy}\frac{\partial^2\delta w_0}{\partial y^2} - M^s_{yy}\frac{\partial^2\delta\varphi}{\partial y^2} + N_{xy}\left(\frac{\partial\delta u_0}{\partial y} + \frac{\partial\delta v_0}{\partial x}\right) - 2M^b_{xy}\frac{\partial^2\delta w_0}{\partial x\partial y} \\ & - 2M^s_{xy}\frac{\partial^2\delta\varphi}{\partial x\partial y} + Q_x\frac{\partial\delta\varphi}{\partial x} + Q_y\frac{\partial\delta\varphi}{\partial y} - q\delta w_0]dA = 0\end{aligned} \tag{10}$$

The definitions of solicitations with N, M, and Q are:

$$(N_{xx}, N_{yy}, N_{xy}) = \int_{-h/2}^{+h/2} \quad (\sigma_{xx}, \sigma_{yy}, \tau_{xy})dZ \tag{11a}$$

$$(M^b_{xx}, M^b_{yy}, M^b_{xy}) = \int_{-h/2}^{+h/2} \quad z.(\sigma_{xx}, \sigma_{yy}, \tau_{xy})dZ \tag{11b}$$

$$(M^s_{xx}, M^s_{yy}, M^s_{xy}) = \int_{-h/2}^{+h/2} \quad f.(\sigma_{xx}, \sigma_{yy}, \tau_{xy})dZ \tag{11c}$$

$$(Q_x, Q_y) = \int_{-h/2}^{+h/2} \quad g.(\tau_{xz}, \tau_{yz})dZ \tag{11d}$$

The transverse loads and the fluctuation of the work done in the plane are given by:

$$\delta V = -\int_A \overline{N}\delta w_0 dA - \int_A q\delta w_0 dA \tag{12}$$

Such as:

$$\overline{N} = N_{xx}^0 \frac{\partial^2 w_0}{\partial x^2} + 2N_{xy}^0 \frac{\partial^2 w_0}{\partial x \partial y} + N_{yy}^0 \frac{\partial^2 w_0}{\partial y^2} \tag{13}$$

The following factors affect how kinetic energy fluctuates:

$$\begin{aligned}
\delta K &= \int_{A}\int_{-h/2}^{+h/2} (\dot{u}\delta\dot{u} + \dot{v}\delta\dot{v} + \dot{w}\delta\dot{w})\rho(z)dAdz \\
&= \int_A \Bigg\{ I_0(\dot{u}_0\delta\dot{u}_0 + \dot{v}_0\delta\dot{v}_0 + \dot{w}_0\delta\dot{w}_0) - I_1(\dot{u}_0\frac{\partial\delta\dot{w}_0}{\partial x} + \frac{\partial\dot{w}_0}{\partial x}\delta\dot{v}_0 + \dot{v}_0\frac{\partial\delta\dot{w}_0}{\partial y} + \frac{\partial\dot{w}_0}{\partial y}\delta\dot{v}_0) \\
&+ I_2\left(\frac{\partial\dot{w}_0}{\partial x}\frac{\partial\delta\dot{w}_0}{\partial x} + \frac{\partial\dot{w}_0}{\partial y}\frac{\partial\delta\dot{w}_0}{\partial y}\right) - J_1\left(\dot{u}_0\frac{\partial\delta\dot{\varphi}}{\partial x} + \frac{\partial\dot{\varphi}}{\partial x}\delta\dot{u}_0 + \dot{v}_0\frac{\partial\delta\dot{\varphi}}{\partial y} + \frac{\partial\dot{\varphi}}{\partial y}\delta\dot{v}_0\right) \\
&+ K_2\left(\frac{\partial\dot{\varphi}}{\partial x}\frac{\partial\delta\dot{\varphi}}{\partial x} + \frac{\partial\dot{\varphi}}{\partial y}\frac{\partial\delta\dot{\varphi}}{\partial y}\right) + J_2\left(\frac{\partial\dot{w}_0}{\partial x}\frac{\partial\delta\dot{\varphi}}{\partial x} + \frac{\partial\dot{\varphi}}{\partial x}\frac{\partial\delta\dot{w}_0}{\partial x} + \frac{\partial\dot{w}_0}{\partial y}\frac{\partial\delta\dot{\varphi}}{\partial y} + \frac{\partial\dot{\varphi}}{\partial y}\frac{\partial\delta\dot{w}_0}{\partial y}\right)\Bigg\} dA
\end{aligned} \tag{14}$$

The mass density denoted by $\boldsymbol{\rho(z)}$, the time variable t is differentiated using the dot-superscript convention, and $\boldsymbol{(I_i, J_i, K_i)}$ are mass inertias.

$$(I_0, I_1, I_2, J_1, J_2, K_2) = \int_{-h/2}^{+h/2} (1, z, z^2, f, zf, f^2)\rho(z)dz \tag{15}$$

Replacing Equation (10), Equation (12), and Equation (14) into Equation (9) and integrating the displacement gradients by parts and setting the coefficients of $\boldsymbol{\partial u_0}$, $\boldsymbol{\partial v_0}$, $\boldsymbol{\partial w_0}$ and $\boldsymbol{\partial \varphi_0}$ to zero separately. The resulting motion equations are as follows:

$$\delta u_0: \frac{\partial N_{xx}}{\partial x} + \frac{\partial N_{xy}}{\partial y} = I_0\ddot{u}_0 - I_1\frac{\partial\ddot{w}_0}{\partial x} - J_1\frac{\partial\ddot{\varphi}}{\partial x} \tag{16a}$$

$$\delta v_0: \frac{\partial N_{xy}}{\partial x} + \frac{\partial N_{yy}}{\partial y} = I_0\ddot{v}_0 - I_1\frac{\partial\ddot{w}_0}{\partial y} - J_1\frac{\partial\ddot{\varphi}}{\partial y} \tag{16b}$$

$$\begin{aligned}
\delta w_0: \frac{\partial^2 M_{xx}^b}{\partial x^2} + 2\frac{\partial^2 M_{xy}^b}{\partial x\partial y} + \frac{\partial^2 M_{yy}^b}{\partial y^2} + \bar{N} + q \\
= I_0\ddot{w}_0 + I_1\left(\frac{\partial\ddot{u}_0}{\partial x} + \frac{\partial\ddot{v}}{\partial y}\right) - I_2\nabla^2\ddot{w}_0 - J_2\nabla^2\ddot{\varphi}
\end{aligned} \tag{16c}$$

$$\delta\varphi_0: \frac{\partial^2 M_{xx}^s}{\partial x^2} + 2\frac{\partial^2 M_{xy}^s}{\partial x \partial y} + \frac{\partial^2 M_{yy}^s}{\partial y^2} + \frac{\partial Q_x}{\partial x} + \frac{\partial Q_y}{\partial y} = J_1\left(\frac{\partial \ddot{u}_0}{\partial x} + \frac{\partial \ddot{v}}{\partial y}\right) - J_2\nabla^2\ddot{w}_0 - K_2\nabla^2\ddot{\varphi} \tag{16d}$$

The stress resultants are given by replacing Equation (6a) with Equation (7) and the findings there form into Equations (11a), (11b), (11c), and (11d).

$$\begin{Bmatrix} N \\ M^b \\ M^s \end{Bmatrix} = \begin{bmatrix} A & B & B^s \\ B & D & D^s \\ B^s & D^s & H^s \end{bmatrix} \begin{Bmatrix} \varepsilon^0 \\ k^b \\ k^s \end{Bmatrix} \tag{17}$$

$$\begin{Bmatrix} Q_x \\ Q_y \end{Bmatrix} = \begin{bmatrix} A_{55}^s & 0 \\ 0 & A_{44}^s \end{bmatrix} \begin{Bmatrix} \gamma_{xz}^0 \\ \gamma_{yz}^0 \end{Bmatrix} \tag{18}$$

where $\boldsymbol{A}, \boldsymbol{A^s}, \boldsymbol{B}, \boldsymbol{D}, \boldsymbol{B^s}, \boldsymbol{D^s}, \boldsymbol{H^s}$ are the plate's stiffness defined by:

$$(A, B, D, B^s, D^s, H^s) = \int_{-h/2}^{+h/2} (1, z, z^2, f, fz, f^2) C(z) dZ \tag{19}$$

$$A_{44}^s = A_{55}^S = \int_{-h/2}^{+h/2} g^2(z) C_{44}(z) dZ = \int_{-h/2}^{+h/2} g^2(z) C_{55}(z) dZ \tag{20}$$

The motion equations can be expressed in the form of displacements. *(u_0, v_0, w_0* et *φ)* by substituting Equations (17 and 18) into Equation (16) as follows:

$$A_{11}\frac{\partial^2 u_0}{\partial x^2} + A_{66}\frac{\partial^2 u_0}{\partial y^2} + (A_{12} + A_{66})\frac{\partial^2 v_0}{\partial x \partial y} - B_{11}\frac{\partial^3 w_0}{\partial x^3} - (B_{12} + 2B_{66})\frac{\partial^2 w_0}{\partial x \partial y^2} - B_{11}^s\frac{\partial^3 \varphi}{\partial x^3} - (B_{12}^s + 2B_{66}^s)\frac{\partial^3 \varphi}{\partial x \partial y^2} = I_0\ddot{u}_0 - I_1\frac{\partial \ddot{w}_0}{\partial x} - J_1\frac{\partial \ddot{\varphi}}{\partial x} \tag{21a}$$

$$A_{22}\frac{\partial^2 v_0}{\partial y^2} + A_{66}\frac{\partial^2 v_0}{\partial x^2} + (A_{12} + A_{66})\frac{\partial^2 u_0}{\partial x \partial y} - B_{22}\frac{\partial^3 w_0}{\partial y^3} - (B_{12} + 2B_{66})\frac{\partial^2 w_0}{\partial x^2 \partial y} - B_{22}^S\frac{\partial^3 \varphi}{\partial y^3} - (B_{12}^s + 2B_{66}^s)\frac{\partial^3 \varphi}{\partial x^2 \partial y} = I_0\ddot{v}_0 - I_1\frac{\partial \ddot{w}_0}{\partial y} - J_1\frac{\partial \ddot{\varphi}}{\partial y} \tag{21b}$$

$$B_{11}\frac{\partial^3 u_0}{\partial x^3}+(B_{12}+2B_{66})\frac{\partial^3 u_0}{\partial x\partial y^2}+(B_{12}2B_{66})\frac{\partial^3 u_0}{\partial x\partial y^2}-D^s_{11}\frac{\partial^4\varphi}{\partial x^4}-D^s_{22}\frac{\partial^4\varphi}{\partial y^4}$$
$$-2(D^s_{12}+2D^s_{66})\frac{\partial^4\varphi}{\partial x^2\partial y^2}+\overline{N}(w)+q \qquad (21c)$$
$$=I_0\ddot{w}_0+I_1\left(\frac{\partial\ddot{u}_0}{\partial x}+\frac{\partial\ddot{v}}{\partial y}\right)-I_2\nabla^2\ddot{w}_0-J_2\nabla^2\ddot{\varphi}$$

$$B^s_{11}\frac{\partial^3 u_0}{\partial x^3}+(B^s{}_{12}+2B^s{}_{66})\frac{\partial^3 u_0}{\partial x\partial y^2}+(B^s{}_{12}+2B^s{}_{66})\frac{\partial^3 v_0}{\partial x^2\partial y}+B^s{}_{66}\frac{\partial^3 v_0}{\partial y^3}$$
$$-D^s_{11}\frac{\partial^4 w_0}{\partial x^4}-D^s_{22}\frac{\partial^4 w_0}{\partial y^4}-2(D^s_{12}+2D^s_{66})\frac{\partial^4 w_0}{\partial x^2\partial y^2}+A^s_{55}\frac{\partial^2\varphi}{\partial x^2}+A^s_{44}\frac{\partial^2\varphi}{\partial y^2} \qquad (21d)$$
$$-D^s_{11}\frac{\partial^4\varphi}{\partial x^4}-H^s_{11}\frac{\partial^4\varphi}{\partial y^4}-2(H^s{}_{12}+2H^s{}_{66})\frac{\partial^3\varphi}{\partial x^2\partial y^2}-H^s_{22}\frac{\partial^4\varphi}{\partial y^4}$$
$$=J_1\left(\frac{\partial\ddot{u}_0}{\partial x}+\frac{\partial\ddot{v}}{\partial y}\right)-J_2\nabla^2\ddot{w}_0-K_2\nabla^2\ddot{\varphi}$$

Analytical Solutions for the FG Plate

The displacement variables are written as a combination of arbitrary parameters and well-known trigonometric functions to ensure that the motion formulas and boundary conditions are respected. The Navier solution method is used for this.

$$\begin{Bmatrix}u_0\\v_0\\w_0\\\varphi\end{Bmatrix}=\sum_{m=1}^{\infty}\sum_{n=1}^{\infty}\begin{Bmatrix}u^0_{mn}\cos(\alpha x)\sin(\beta y)e^{i\omega t}\\v^0_{mn}\sin(\alpha x)\cos(\beta y)e^{i\omega t}\\x^0_{mn}\sin(\alpha x)\sin(\beta y)e^{i\omega t}\\y^0_{mn}\sin(\alpha x)\sin(\beta y)e^{i\omega t}\end{Bmatrix} \qquad (22)$$

$$\alpha=m\pi/a\,,\quad \beta=n\pi/b \qquad (23)$$

The double Fourier sinus series expands the transverse force $\boldsymbol{q}$ as well:

$$q(x,y)=\sum_{m=1}^{\infty}\sum_{n=1}^{\infty}q_{mn}\sin(\alpha x)\sin(\beta y)e^{i\omega t} \qquad (24)$$

$\boldsymbol{\alpha}$ and $\boldsymbol{\beta}$ are natural numbers, $\boldsymbol{a}$ and $\boldsymbol{b}$ are the dimensions of the plate according to the $\boldsymbol{x}$ and $\boldsymbol{y}$ axes, correspondingly, $\boldsymbol{q_{mn}=q_0}$ for a load with a

sinusoidal distribution. Taking into account that the plate is experiencing a compressive load in its plane:

$$N_{xx}^0 = -N_0, N_{yy}^0 = -\gamma N_0 \; N_{xy}^0 = 0,$$

γ is a non-dimensional load parameter. Substituting Equation (22) into Equation (21), it's discovered the problem:

$$\left(\begin{bmatrix} s_{11} & s_{12} & s_{13} & s_{14} \\ s_{12} & s_{22} & s_{23} & s_{24} \\ s_{13} & s_{23} & s_{33}+\lambda & s_{34} \\ s_{14} & s_{24} & s_{34} & s_{44} \end{bmatrix} - w^2 \begin{bmatrix} m_{11} & 0 & m_{13} & m_{14} \\ 0 & m_{22} & m_{23} & m_{24} \\ m_{13} & m_{23} & m_{33} & m_{34} \\ m_{14} & m_{24} & m_{34} & m_{44} \end{bmatrix} \right) \begin{Bmatrix} u_{mn}^0 \\ v_{mn}^0 \\ x_{mn}^0 \\ y_{mn}^0 \end{Bmatrix} = \begin{Bmatrix} 0 \\ 0 \\ q_{mn} \\ 0 \end{Bmatrix} \quad (25)$$

where:

$$s_{11} = A_{11}\alpha^2 + A_{66}\beta^2, s_{12} = (A_{11} + A_{66})\alpha\beta, s_{13} = -B_{11}\alpha^3 - (B_{12} + 2B_{66})\alpha\beta^2,$$

$$s_{14} = -B_{11}^s\alpha^3 - (B_{12}^s + 2B_{66}^s)\alpha\beta^2, s_{22} = A_{66}\alpha^2 + A_{22}\beta^2,$$

$$s_{23} = -B_{22}\beta^3 - (B_{12} + 2B_{66})\alpha^2\beta, s_{24} = -B_{22}^s\beta^3 - (B_{12}^s + 2B_{66}^s)\alpha^2\beta,$$

$$s_{33} = D_{11}\alpha^4 + 2(D_{12} + 2D_{66})\alpha^2\beta^2 + D_{22}\beta^4,$$

$$s_{34} = D_{11}^s\alpha^4 + 2(D_{12}^s + 2D_{66}^s)\alpha^2\beta^2 + D_{22}^s\beta^4, \quad (26)$$

$$s_{44} = H_{11}^s\alpha^4 + 2(H_{12}^s + 2H_{66}^s)\alpha^2\beta^2 + H_{22}^s\beta^4 + A_{55}^s\alpha^2 + A_{44}^s\beta^2,$$

$$m_{11} = m_{22} = I_0, m_{13} = -\alpha I_1, m_{14} = -\alpha J_1, m_{23} = -\beta I_1, m_{24} = -\beta J_1,$$

$$m_{33} = I_0 + I_2(\alpha^2 + \beta^2), m_{34} = J_2(\alpha^2 + \beta^2), m_{44} = K_2(\alpha^2 + \beta^2)$$

$$\lambda = -N_0(\alpha^2 + \gamma\beta^2).$$

Numerical example

We study a rectangular, simply supported FG plate with dimensions a and b, located, respectively, in the x- and y-axes (see Figure 1). In Table 2, the material qualities are listed.

Table 2: Qualities of plate materials

Material	Young's modulus (GPa)	Mass density (kg/m^3)	Poisson's ratio
Aluminium (Al)	70	2.702	0.3
Alumina (Al_2O_3)	380	3.800	0.3
Zirconia (ZrO_2)	151	3.000	0.3
Silicon carbide (SiC)	420	3.210	0.3

The accuracy of the current analysis is examined in the section that follows, which also examines the effects of the geometric ratio and the power-law index on the deflections, stresses, and critical buckling loads of FG plates. The following dimensionless parameters are chosen because they are more practical:

$$\overline{u} = \frac{100E_c h^3}{q_0 a^4} u\left(0, \frac{b}{2}, z\right), \overline{w} = \frac{10E_c h^3}{q_0 a^4} w\left(\frac{a}{2}, \frac{b}{2}\right) \tag{27}$$

$$\overline{\sigma}_{xx}(z) = \frac{h}{q_0 a} \sigma_{xx}\left(\frac{a}{2}, \frac{b}{2}, z\right), \overline{\tau}_{xy}(z) = \frac{h}{q_0 a} \sigma_{xy}(0,0,z), \tag{28}$$

$$\overline{\tau}_{xz}(z) = \frac{h}{q_0 a} \sigma_{xz}\left(0, \frac{b}{2}, z\right)$$

$$\widehat{N}_{cr} = \frac{N_{cr} a^2}{D_{11} - \left(B_{11}^2 / A_{11}\right)}, \overline{N}_{cr} = \frac{N_{cr} a^2}{E_m h^3} \tag{29}$$

Bending analysis

To check the accuracy of the proposed model in investigating the bending, Tables 3 (square plates, *h/a*=0.1) and 4 determine the central deflections, transverse shear stresses, and normal stresses of plates (Al/Al2O3) under sinusoidal loads. The outcomes of several shear deformation theories were compared, including quasi-3D, 3D, sinusoidal shear deformation theory (SSDT), third-order shear deformation theory (TSDT), and those that took into account both transverse shear and normal stresses. It can be seen from these results that the computations based on the present 2D (HSDT) theory present an excellent agreement with those predicted by the other theories of TSDT [33] and HSDT [34] and present a good correlation with those predicted by Quasi-3D [35], Quasi-3D [36], SSDT [37], and HSDT [38].

Table 3: Dimensionless $(\bar{u}, \bar{w}, \bar{\sigma}_{xx}, \bar{\tau}_{xy}, \bar{\tau}_{xz})$ of square plates (Al/Al_2O_3)

p	Theory	$\bar{u}(-h/4)$	$\bar{w}$	$\bar{\sigma}_{xx}(h/3)$	$\bar{\tau}_{xy}(-h/3)$	$\bar{\tau}_{xz}(h/6)$
1	Quasi-3D [35]	0.6436	0.5875	1.5062	0.6081	0.2510
	Quasi-3D [36]	0.6436	0.5876	1.5061	0.6112	0.2511
	SSDT [37]	0.6626	0.5889	1.4894	0.6110	0.2622
	HSDT [38]	0.6398	0.5880	1.4888	0.6109	0.2566
	TSDT [33]	0.6414	0.5890	1.4898	0.6111	0.2599
	HSDT [34]	0.6414	0.5891	1.4898	0.6111	0.2608
	HSDT [39]	0.6401	0.5883	1.4892	0.6110	0.2552
	Present	0.6414	0.5890	1.4898	0.6111	0.2608
2	Quasi-3D [35]	0.9012	0.7570	1.4147	0.5421	0.2496
	Quasi-3D [36]	0.9013	0.7571	1.4133	0.5436	0.2495
	SSDT [37]	0.9281	0.7573	1.3954	0.5441	0.2763
	HSDT [38]	0.8957	0.7564	1.3940	0.5438	0.2741
	TSDT [33]	0.8984	0.7573	1.3960	0.5442	0.2721
	HSDT [34]	0.8984	0.7573	1.3960	0.5442	0.2721
	HSDT [39]	0.8961	0.7567	1.3947	0.5439	0.2721
	Present	0.8984	0.7573	1.3960	0.5442	0.2737
4	Quasi-3D [35]	1.0541	0.8823	1.1985	0.5666	0.2362
	Quasi-3D [36]	1.0541	0.8823	1.1841	0.5671	0.2362
	SSDT [37]	1.0941	0.8819	1.1783	0.5667	0.2580
	HSDT [38]	1.0457	0.8814	1.1755	0.5662	0.2623
	TSDT [33]	1.0502	0.8815	1.1794	0.5669	0.2519
	HSDT [34]	1.0502	0.8815	1.1794	0.5669	0.2537
	HSDT [39]	1.0466	0.8818	1.1766	0.5664	0.2593
	Present	1.0502	0.8815	1.1794	0.5669	0.2537
8	Quasi-3D [35]	1.0830	0.9739	0.9687	0.5879	0.2262
	Quasi-3D [36]	1.0830	0.9739	0.9687	0.5879	0.2261
	SSDT [37]	1.1340	0.9750	0.9466	0.5856	0.2121
	HSDT [38]	1.0709	0.9737	0.9431	0.5850	0.2140
	TSDT [33]	1.0763	0.9747	0.9477	0.5858	0.2087
	HSDT [34]	1.0763	0.9746	0.9477	0.5858	0.2088
	HSDT [39]	1.0719	0.9744	0.9444	0.5852	0.2117
	Present	1.0763	0.9746	0.9477	0.5858	0.2088

The variations in-plane displacement, normal and tangential stresses across the thickness of the square plate (Al/Al_2O_3) are shown in Figure 2. It can be seen that the lower part of the plate is in tension and the upper part. In compression, the dimensionless displacement increased with the increase in the power index, and was equal to zero, for (z/h= 0).

Table 4: Dimensionless deflection ($\bar{W}$) of plates (Al/Al_2O_3)

h/a	*a/b*	Theory	*p*					
			0.1	0.3	0.5	0.7	1	1.5
0.5	1	3D [24]	0.576	0.524	0.476	0.432	0.372	0.289
		Quasi-3D	0.573	0.518	0.467	0.422	0.361	0.277
		Quasi-3D	0.577	0.522	0.471	0.425	0.364	0.279
		HSDT [38]	0.636	0.575	0.519	0.468	0.401	0.307
		HSDT [34]	0.636	0.575	0.519	0.468	0.401	0.307
		HSDT [39]	0.621	0.561	0.507	0.457	0.392	0.301
		Present	0.619	0.575	0.519	0.468	0.399	0.305
	0.5	3D [24]	1.194	1.085	0.986	0.895	0.772	0.601
		Quasi-3D	1.188	1.074	0.970	0.875	0.749	0.575
		Quasi-3D	1.193	1.079	0.974	0.879	0.753	0.578
		HSDT [38]	1.277	1.155	1.044	0.943	0.809	0.623
		HSDT [34]	1.277	1.155	1.044	0.943	0.808	0.623
		HSDT [39]	1.256	1.136	1.027	0.928	0.796	0.615
		Present	1.256	1.155	1.043	0.942	0.807	0.621
	0.3	3D [24]	1.443	1.311	1.191	1.081	0.933	0.727
	3	Quasi-3D	1.435	1.297	1.172	1.058	0.905	0.696
		Quasi-3D	1.441	1.303	1.177	1.062	0.909	0.699
		HSDT [38]	1.534	1.387	1.254	1.132	0.972	0.750
		HSDT [34]	1.534	1.387	1.254	1.132	0.971	0.750
		HSDT [39]	1.511	1.367	1.236	1.116	0.958	0.741
		Present	1.510	1.387	1.253	1.132	0.971	0.749
0.2	1	3D [24]	0.349	0.316	0.287	0.260	0.225	0.180
5		Quasi-3D	0.347	0.314	0.283	0.256	0.219	0.169
		Quasi-3D	0.348	0.315	0.284	0.257	0.220	0.169
		HSDT [38]	0.360	0.325	0.294	0.266	0.229	0.178
		HSDT [34]	0.360	0.325	0.294	0.266	0.229	0.178
		HSDT [39]	0.357	0.323	0.292	0.264	0.228	0.177
		Present	0.359	0.326	0.295	0.267	0.230	0.180
	0.5	3D [24]	0.815	0.739	0.670	0.608	0.525	0.412
		Quasi-3D	0.812	0.734	0.663	0.599	0.513	0.396
		Quasi-3D	0.814	0.736	0.665	0.600	0.515	0.397
		HSDT [38]	0.832	0.753	0.681	0.617	0.531	0.415
		HSDT [34]	0.832	0.753	0.681	0.617	0.531	0.415
		HSDT [39]	0.828	0.749	0.678	0.614	0.529	0.413
		Present	0.831	0.753	0.681	0.617	0.531	0.413
	0.3	3D [24]	1.013	0.919	0.833	0.756	0.653	0.512
	3	Quasi-3D	1.009	0.912	0.824	0.744	0.638	0.492
		Quasi-3D	1.012	0.915	0.827	0.747	0.640	0.494
		HSDT [38]	1.032	0.934	0.845	0.765	0.660	0.515
		HSDT [34]	1.032	0.934	0.845	0.765	0.660	0.515
		HSDT [39]	1.028	0.930	0.842	0.762	0.657	0.513
		Present	1.031	0.934	0.845	0.765	0.659	0.514

Concerning the greatest axial tension rises as the power index *p* whereas it appears minimal compressed stresses positioned at the lower part

of the plate intended certain values of p (p=0, $\bar{\sigma}_{xx} = -2$ and p=0.5, $\bar{\sigma}_{xx} = -0.65$) the axial stress is in tension in the upper part (p=0,$\bar{\sigma}_{xx} = 2$ and p=40, $\bar{\sigma}_{xx} = 8.07$).

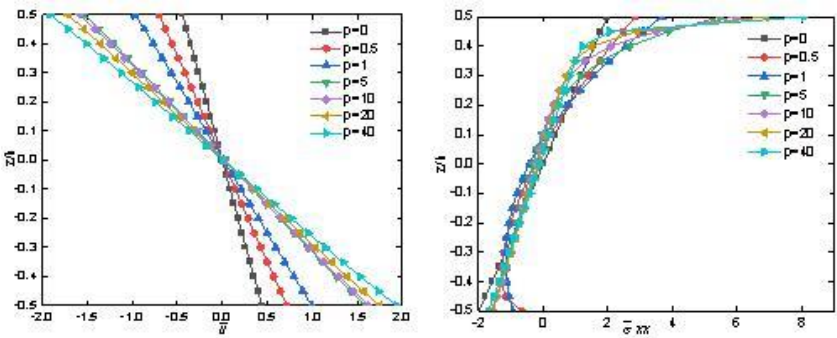

Figure 2: In-plane displacement ($\bar{u}$) and stress ($\bar{\sigma}_{xx}$)along the thickness of Al/Al_2O_3 square plates (h/a=0.1)

Figure 3 displays the change in tangential cross-thickness stresses on the FG plate, for homogeneous plates, the mid-plane is where the highest shear stress is located, and it tends to migrate slightly to the top surface, this is an asymmetric characteristic of the FGM through the thickness of the FG plate.

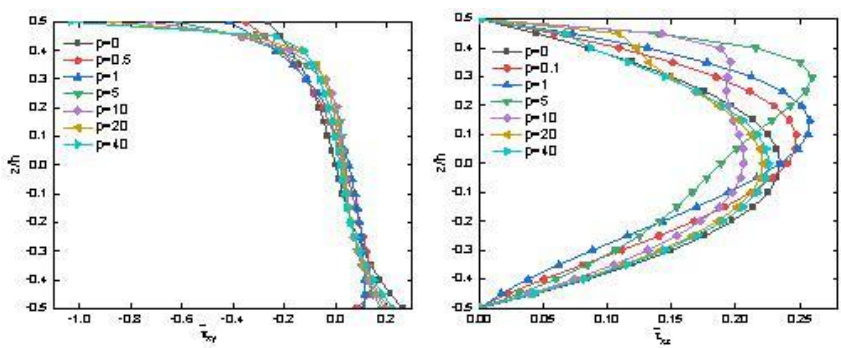

Figure 3: In-plane stress ($\bar{\tau}_{xy}$) and ($\bar{\tau}_{xz}$) long the thickness of Al/Al_2O_3 square plates (h/a=0.5)

Buckling analysis

Calculated critical buckling loads and compared them to those accessible in the literature to assess the efficacy of the current results in forecasting a

buckling response of FG plates. The following example investigates the buckling reactions of Al/Al2O3 and Al/SiC plates under three different types of in-plane loads: uniaxial compression, biaxial compressions, axial compression, and tension (γ=0), (γ=1), and (γ=-1), respectively. Because of differences in material characteristics over the thickness, stretching-bending coupling arises in FG plates.

Table 5: The critical buckling load ($\hat{N}cr$) of Al/SiC square plates (*h/a*=0.1)

γ	Theory	*p*					
		0	0.5	1	2	5	10
0	HSDT [39]	37.4215	37.6650	37.7560	37.6327	36.8862	36.5934
	FSDT [42]	37.3708	-	37.7132	37.7089	-	-
	HSDT [20]	37.3714	-	37.7172	37.5765	-	-
	HSDT [43]	37.3721	-	37.7143	37.6042	-	-
	Present	37.3721	37.6302	37.7143	37.6042	36.9183	36.5615
1	HSDT [39]	18.7107	18.8325	18.8780	18.8163	18.4431	18.2967
	FSDT [42]	18.6854	-	18.8566	18.8545	-	-
	HSDT [20]	18.6860	-	18.8571	18.8020	-	-
	HSDT [43]	18.6861	-	18.8572	18.8021	-	-
	Present	18.6861	18.8151	18.8572	18.8021	18.4591	18.2807
-1	HSDT [39]	72.3281	73.4526	73.8426	73.2827	69.9876	68.7244
	FSDT [42]	72.0834	-	73.6307	73.6112	-	-
	HSDT [20]	72.2275	-	73.6645	73.1587	-	-
	HSDT [43]	72.0983	-	73.6437	73.1436	-	-
	Present	72.0983	73.5127	74.2938	74.2403	71.0104	69.0775

When the plate is subjected to in-plane compressive loads, this coupling induces deflection and bending moments.

The results of Table 5 present the critical buckling load of a simply supported square plate (Al/SiC) with a constant geometric ratio (*h/a*=0.1). The outcomes are contrasted with those. of the HSDT [39], FSDT [42], HSDT [20], and HSDT [43]. The computed results have good accuracy for square plates.

To further illustrate the accuracy of the present theory for a wide range of thickness ratio (*a/h*), geometric ratio *(b/a)*, different values of gradient index *(p),* and different cases of the dimensionless load parameter ($\boldsymbol{\gamma}$), comparison of the variations of critical buckling load ($\bar{N}cr$) of Al/Al2O3 plates computed by the present theory, HSDT [43] and HSDT [39] is presented in Table 6, as seen in the table, there is a good agreement between the computed results from the proposed theory and the computed results from other HSDT.

Table 6: The critical buckling load ($\bar{N}$cr) of Al/Al2O3 plates

γ	b/a	h/a	Theory	p					
				0	0.5	1	2	5	10
0	2	0.2	HSDT[43]	6.7203	4.4235	3.4164	2.6451	2.1484	1.9213
			HSDT[39]	6.7417	4.4343	3.4257	2.6503	2.1459	1.9260
			Present	6.7203	4.4235	3.4164	2.6451	2.1484	1.9213
		0.1	HSDT[43]	7.4053	4.8206	3.7111	2.8897	2.4165	2.1896
			HSDT[39]	7.4115	4.8225	3.7137	2.8911	2.4155	2.1911
			Present	7.4053	4.8206	3.7111	2.8897	2.4165	2.1896
		0.05	HSDT[43]	7.5993	4.9315	3.7930	2.9382	2.4944	2.2690
			HSDT[39]	7.6009	4.9307	3.7937	2.9585	2.4942	2.2695
			Present	7.5993	4.9315	3.7930	2.9582	2.4944	2.2690
	1	0.2	HSDT[43]	16.0211	10.6254	8.2245	6.3432	5.0531	4.4807
			HSDT[39]	16.1003	10.6670	8.2597	6.3631	5.0459	4.4981
			Present	16.0211	10.4629	7.9086	5.94263	4.7928	4.355
		0.1	HSDT[43]	18.5785	12.1229	9.3391	7.2631	6.0353	5.4528
			HSDT[39]	18.6030	12.1317	9.3496	7.2687	6.0316	5.4587
			Present	18.5785	11.9128	8.9338	6.7404	5.6678	5.2707
		0.05	HSDT[43]	19.3528	12.5668	9.6675	7.5371	6.3448	5.7668
			HSDT[39]	19.3593	1.25652	9.6702	7.5386	6.3437	5.7689
			Present	19.3528	12.3413	9.2339	6.9752	5.9399	5.5643
1	2	0.2	HSDT[43]	5.3762	3.5388	2.7331	2.1161	1.7187	1.5370
			HSDT[39]	5.3934	3.5475	2.7406	2.1202	1.7167	1.5408
			Present	5.3762	3.5388	2.7331	2.1161	1.7187	1.5370
		0.1	HSDT[43]	5.9243	3.8565	2.7689	2.3117	1.9332	1.7517
			HSDT[39]	5.9292	3.8580	2.9710	2.3129	1.9324	1.7529
			Present	5.9243	3.8565	2.9689	2.3117	1.9332	1.7517
		0.05	HSDT[43]	6.0794	3.9452	3.0344	2.3665	1.9955	1.8152
			HSDT[39]	6.0807	3.9445	3.0350	2.3668	1.9953	1.8156
			Present	6.0794	3.9452	3.0344	2.3665	1.9955	1.8152
	1	0.2	HSDT[43]	8.0105	5.3127	4.1122	3.1716	2.5265	2.2403
			HSDT[39]	8.0501	5.3335	4.1299	3.1815	2.5230	2.2491
			Present	8.0105	5.2314	3.9543	2.9713	2.3964	2.1775
		0.1	HSDT[43]	9.2893	6.0615	.46696	3.6315	3.0177	2.7264
			HSDT[39]	9.3015	6.0659	4.6748	3.6344	3.0158	2.7293
			Present	9.2893	5.9564	4.4669	3.3702	2.8339	2.6354
		0.05	HSDT[43]	9.6764	6.2834	4.8337	3.7686	3.1724	2.8834
			HSDT[39]	9.6796	6.2826	4.8351	3.7693	3.1718	2.8844
			Present	9.6764	6.1706	4.6169	3.4876	2.9699	2.7821
1	2	0.2	HSDT[43]	8.9604	5.8980	4.5551	3.5268	2.8646	2.5617
			HSDT[39]	8.9890	5.9124	4.5676	3.5337	2.8612	2.5679
			Present	8.9604	5.8980	4.5551	3.5268	2.8646	2.5617
		0.1	HSDT[43]	9.8738	6.4275	4.9481	3.8529	3.2219	2.9195

		HSDT[39]	9.8820	6.4299	4.9516	3.8548	3.2206	2.9214
		Present	9.8738	6.4275	4.9481	3.8529	3.2219	2.9195
	0.05	HSDT[43]	10.1324	6.5753	5.0574	3.9442	3.3259	3.0253
		HSDT[39]	10.1345	6.5742	5.0583	3.9447	3.3255	3.0260
		Present	10.1324	6.5753	5.0574	3.9442	3.3259	3.0253
1	0.2	HSDT[43]	26.2058	17.7704	13.8486	10.5589	16.9590	6.8970
		HSDT[39]	24.4999	17.9424	13.9872	10.6421	7.9571	6.9626
		Present[a]	26.2058	17.7947	13.8958	10.6164	7.9927	6.9132
	0.1	HSDT[43]	35.8416	23.5920	18.2206	14.1073	11.4583	10.2468
		HSDT[39]	35.9559	23.6497	18.2704	14.1349	11.4447	10.2717
		Present[a]	35.8416	23.6343	18.3023	14.2113	11.5283	10.2812
	0.05	HSDT[43]	39.4951	25.7100	19.7925	15.4115	12.8878	11.6779
		HSDT[39]	39.5280	25.7197	19.8065	15.4190	12.8824	11.6857
		Present[a]	39.4951	25.7602	19.8890	15.5361	12.9764	11.7220

[a] Critical buckling

In Figure 6(a), the buckling responses of the Al/Al_2O_3 plate, are studied for three types of loads in the plane considered: ($\gamma=0$), ($\gamma=-1$), and ($\gamma=1$). For the three cases, for the power-law index ($P=0$) the essential buckling load, in terms of value ($\bar{N}cr$) is maximum, then with the increase in (p) will decrease the critical load ($\bar{N}cr$).

A variety of thickness to the ratio *(a /h)*, varying gradient index values (p), and for ($\gamma=1$), the value of the critical buckling load ($\bar{N}$cr) is maximum for ($p=0$), then after certain values of (a/h), the curves remain flat, as plotted in Figure 6(b).

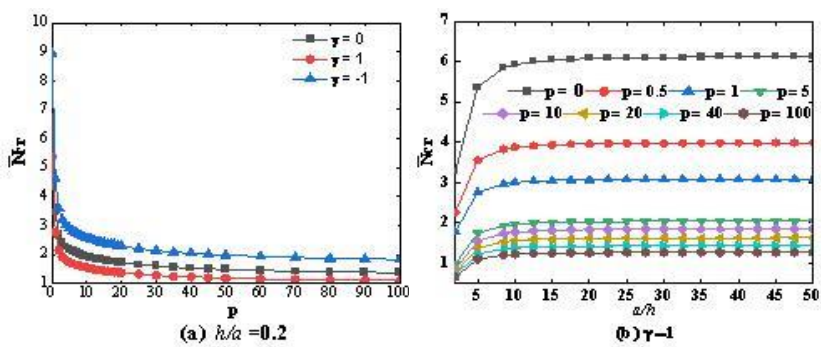

Figure 6: The critical buckling load ($\bar{N}$cr) of rectangular plates (Al/Al_2O_3) ($b/a=2$) is affected by the power-law index p and side-to-thickness ratio ($a=0.9h$)

Conclusion

The current study uses a novel 2D HSDT to analyse the buckling and bending of simply supported FG plates. By developing a new shear deformation shape function, the theory is constructed. Hamilton's rule is used to generate equations describing motion. Navier's technique is used to resolve these equations. The results were compared to those given by several plate theories for the novel shear deformation shape function employed in this work. As a consequence, when compared to the FSDT and other HSDTs with a greater number of unknowns, the created HSDT delivers findings with extremely good accuracy. As a result, the current model may be used as a benchmark to evaluate the effectiveness of approximative numerical methods.

Contributions of Authors

The author confirms that this work is individual. the author reviewed , and approved the final version of this work.

Funding

This work received no specific grant from any funding agency.

Conflict of Interests

The author declares that they have no conflicts of interest.

References

[1] M. Koizumi, "FGM activities in Japan", *Composites. Part B Engineering*, vol. 28, no. 1–2, pp. 1–4, 1997.
[2] D. K. Jha, T. Kant, and R. K. Singh, "Free vibration response of functionally graded thick plates with shear and normal deformations effects", *Composite Structures*, vol. 96, pp. 799–823, 2013. doi: 10.1016/j.compstruct.2012.09.034.
[3] G. Kirchhoff, "Über das gleichgewicht und die bewegung einer elastischen scheibe", *Journal Für Die Reine Und Angewandte Mathematik (Crelles Journal)*, vol. 1850, no. 40, pp. 51–88, 1850.
[4] J. Cugnoni, "Identification par decalage modal et fréquentiel en

matériaux composites", Ph.D dissertation, Faculty of Eng., Federal Ins. of Tech., Lausanne, 2005. [Online]. Available: https://core.ac.uk/download/pdf/147900375.pdf

[5] E. Reissner, "The effect of transverse shear deformation on the bending of elastic plates", *Journal of Applied Mechanics*, vol. 12, no. 2, pp. A69–A77, 1945. doi: 10.1115/1.4009435.

[6] Q. Zhang, S. Li, A. Zhang, Y. Peng, and J. Yan, "A peridynamic Reissner-Mindlin shell theory", *International Journal for Numerical Methods in Engineering*, vol. 122, no. 1, pp. 122–147, 2021. doi: 10.1002/nme.6527.

[7] Z. Kolakowski and J. Jankowski, "Some inconsistencies in the nonlinear buckling plate theories—fsdt, s-fsdt, hsdt", *Materials (Basel).*, vol. 14, no. 9, pp. 1-20, 2021. doi: 10.3390/ma14092154.

[8] C.-U. Nguyen, J.-L. Batoz, and A. Ibrahimbegovic, "Notable highlights on locking-free techniques of Reissner-Mindlin plate finite elements in elastostatics", *Coupled System Mechanics An International Journal*, vol. 10, no. 3, pp. 229–246, 2021. doi: https://doi.org/10.12989/csm.2021.10.3.229.

[9] J. Videla, S. Natarajan, and S. P. A. Bordas, "A new locking-free polygonal plate element for thin and thick plates based on Reissner-Mindlin plate theory and assumed shear strain fields", *Computers & Structures*, vol. 220, pp. 32–42, 2019. doi: 10.1016/j.compstruc.2019.04.009.

[10] A. Bhar, S. S. Phoenix, and S. K. Satsangi, "Finite element analysis of laminated composite stiffened plates using FSDT and HSDT: A comparative perspective", *Composite Structures*, vol. 92, no. 2, pp. 312–321, Jan. 2010. doi: 10.1016/j.compstruct.2009.08.002.

[11] A. Tounsi, H. Ait Atmane, M. Khiloun, M. Sekkal, O. Taleb, and A. Anis Bousahla, "On buckling behaviour of thick advanced composite sandwich plates", *Composite Materials and Engineering*, vol. 1, no. 1, pp. 1–19, 2019. https://doi.org/10.12989/cme.2019.1.1.001.

[12] A. Bouhadra, A. Tounsi, A. A. Bousahla, S. Benyoucef, and S. R. Mahmoud, "Improved HSDT accounting for effect of thickness stretching in advanced composite plates", *Structural Engineering and Mechanics*, vol. 66, no. 1, pp. 61–73, 2018. doi: https://doi.org/10.12989/sem.2018.66.1.061.

[13] F. Tornabene, N. Fantuzzi, M. Bacciocchi, and E. Viola, "Mechanical behaviour of damaged laminated composites plates and shells: Higher-order Shear Deformation Theories", *Composite Structures*, vol. 189, pp. 304–329, Apr. 2018. doi: 10.1016/j.compstruct.2018.01.073.

[14] Z. Q. Cheng and R. C. Batra, "Deflection relationships between the homogeneous Kirchhoff plate theory and different functionally graded plate theories", *Archives of Mechanics*, vol. 52, no. 1, pp. 143–158, 2000.

[15] E. Cheshmeh, M. Karbon, A. Eyvazian, D. won Jung, M. Habibi, and M. Safarpour, “Buckling and vibration analysis of FG-CNTRC plate subjected to thermo-mechanical load based on higher order shear deformation theory”, *Mechanics Based Design Structures and Machines*, vol. 50, no. 4, pp. 1137–1160, 2022. doi: 10.1080/15397734.2020.1744005.

[16] K. Kulkarni, B. N. Singh, and D. K. Maiti, “Analytical solution for bending and buckling analysis of functionally graded plates using inverse trigonometric shear deformation theory”, *Composite Structures*, vol. 134, pp. 147–157, 2015. doi: 10.1016/j.compstruct.2015.08.060.

[17] B. A. S. Shariat, R. Javaheri, and M. R. Eslami, “Buckling of imperfect functionally graded plates under in-plane compressive loading”, Thin-Walled Structures, vol. 43, no. 7, pp. 1020–1036, 2005. doi: 10.1016/j.tws.2005.01.002.

[18] S. Abrate, “Free vibration, buckling, and static deflections of functionally graded plates”, *Composites Science and Technology*, vol. 66, no. 14, pp. 2383–2394, 2006. doi: 10.1016/j.compscitech.2006.02.032.

[19] I. Mechab, H. A. Atmane, A. Tounsi, H. A. Belhadj, and E. A. A. Bedia, “A two variable refined plate theory for the bending analysis of functionally graded plates”, *Acta Mechanica Sinica*, vol. 26, no. 6, pp. 941–949, Dec. 2010. doi: 10.1007/s10409-010-0372-1.

[20] M. Bodaghi and A. R. Saidi, “Levy-type solution for buckling analysis of thick functionally graded rectangular plates based on the higher-order shear deformation plate theory”, *Applied Mathematical Modelling*, vol. 34, no. 11, pp. 3659–3673, 2010. doi: 10.1016/j.apm.2010.03.016.

[21] M. Bourada and E. A. Adda Bedia, “Analyse du flambement des structures hétérogènes sandwiches sous chargement thermique en utilisant les théories à ordre élevé”, 2013.

[22] T. Becheri, K. Amara, M. Bouazza, and N. Benseddiq, “Buckling of symmetrically laminated plates using nth-order shear deformation theory with curvature effects”, *Steel and Composite Structures*, vol. 21, no. 6, pp. 1347–1368, 2016. doi: 10.12989/scs.2016.21.6.1347.

[23] J. L. Pelletier and S. S. Vel, “An exact solution for the steady-state thermoelastic response of functionally graded orthotropic cylindrical shells”, *International Journal of Solids and Structures*, vol. 43, no. 5, pp. 1131–1158, 2006. doi: 10.1016/j.ijsolstr.2005.03.079.

[24] A. M. Zenkour, “Benchmark trigonometric and 3-D elasticity solutions for an exponentially graded thick rectangular plate”, *Archive Applied Mechanics*, vol. 77, no. 4, pp. 197–214, Feb. 2007. doi: 10.1007/s00419-006-0084-y.

[25] S. A. Ambartsumyan, “Theory of anisotropic plate”, *Technomic Publication Company*, 1969.

[26] K. Soldatos, “A transverse shear deformation theory for homogeneous

monoclinic plates," *Acta Mechanica*, vol. 94, no. 3, pp. 195–220, 1992.
[27] M. Touratier, "An efficient standard plate theory", *International Journal of Engineering Science*, vol. 29, no. 8, pp. 901–916, 1991. doi: 10.1016/0020-7225(91)90165-Y.
[28] M. Karama, K. S. Afaq, and S. Mistou, "Mechanical behaviour of laminated composite beam by the new multi-layered laminated composite structures model with transverse shear stress continuity", *International Journal Solids Structure*, vol. 40, no. 6, pp. 1525–1546, 2003. doi: 10.1016/S0020-7683(02)00647-9.
[29] N. Grover, D. K. Maiti, and B. N. Singh, "A new inverse hyperbolic shear deformation theory for static and buckling analysis of laminated composite and sandwich plates", *Composite Structures*, vol. 95, pp. 667–675, Jan. 2013. doi: 10.1016/j.compstruct.2012.08.012.
[30] A. Benbakhti, M. B. Bouiadjra, N. Retiel, and A. Tounsi, "A new five unknown quasi-3D type HSDT for thermomechanical bending analysis of FGM sandwich plates", *Steel and Composite Structures*, vol. 22, no. 5, pp. 975–999, Dec. 2016. doi: 10.12989/scs.2016.22.5.975.
[31] A. Meftah, A. Bakora, F. Z. Zaoui, A. Tounsi, and E. A. A. Bedia, "A non-polynomial four variable refined plate theory for free vibration of functionally graded thick rectangular plates on elastic foundation", *Steel and Composite Structures*, vol. 23, no. 3, pp. 317–330, 2017. doi: 10.12989/scs.2017.23.3.317.
[32] J. N. Reddy, "Analysis of functionally graded plates", *International Journal Numerical Methods in Engineering*, vol. 47, no. 1-3, pp. 663-684, 2000. doi: 10.1002/(SICI)1097-0207(20000110/30)47:1/3<663::AID-NME787>3.0.CO;2-8.
[33] C.-P. P. Wu and H.-Y. Y. Li, "An RMVT-based third-order shear deformation theory of multilayered functionally graded material plates", *Composite Structures*, vol. 92, no. 10, pp. 2591–2605, 2010. doi: 10.1016/j.compstruct.2010.01.022.
[34] H.-T. Thai and D.-H. Choi, "A simple first-order shear deformation theory for the bending and free vibration analysis of functionally graded plates", *Composite Structures*, vol. 101, pp. 332–340, 2013. doi: 10.1016/j.compstruct.2013.02.019.
[35] E. Carrera, S. Brischetto, and A. Robaldo, "Variable Kinematic Model for the Analysis of Functionally Graded Material plates", *AIAA Journal*, vol. 46, no. 1, pp. 194–203, Jan. 2008. doi: 10.2514/1.32490.
[36] C.-P. Wu, K.-H. Chiu, and Y.-M. Wang, "RMVT-based meshless collocation and element-free Galerkin methods for the quasi-3D analysis of multilayered composite and FGM plates, *Composite Structures*, vol. 93, no. 2, pp. 923–943, 2011. doi: 10.1016/j.compstruct.2010.07.001.
[37] A. M. Zenkour, "Generalized shear deformation theory for bending analysis of functionally graded plates", *Applied Mathematical*

Modelling, vol. 30, no. 1, pp. 67–84, 2006. doi: 10.1016/j.apm.2005.03.009.
[38] J. L. L. Mantari, A. S. Oktem, C. Guedes Soares, and C. G. Soares, "Bending response of functionally graded plates by using a new higher order shear deformation theory", *Composite Structures*, vol. 94, no. 2, pp. 714–723, 2012. doi: 10.1016/j.compstruct.2011.09.007.
[39] T.-K. K. Nguyen, "A higher-order hyperbolic shear deformation plate model for analysis of functionally graded materials", *International Journal Mechanics and Materials in Design*, vol. 11, no. 2, pp. 203–219, May 2015. doi: 10.1007/s10999-014-9260-3.
[40] A. M. Zenkour, "A simple four-unknown refined theory for bending analysis of functionally graded plates", *Applied Mathematical Modelling*, vol. 37, no. 20–21, pp. 9041–9051, 2013. doi: 10.1016/j.apm.2013.04.022.
[41] J. L. Mantari and C. Guedes Soares, "Generalized hybrid quasi-3D shear deformation theory for the static analysis of advanced composite plates", *Composite Structures*, vol. 94, no. 8, pp. 2561–2575, 2012. doi: 10.1016/j.compstruct.2012.02.019.
[42] M. Mohammadi, A. R. Saidi, and E. Jomehzadeh, "A novel analytical approach for the buckling analysis of moderately thick functionally graded rectangular plates with two simply-supported opposite edges", *Proceedings of the Institution of Mechanical Engineers, Part C: Journal Mechanical Engineering Science*, vol. 224, no. 9, pp. 1831–1841, 2010. doi: 10.1243/09544062JMES1804.
[43] H.-T. Thai and D.-H. Choi, "An efficient and simple refined theory for buckling analysis of functionally graded plates", *Applied Mathematical Modelling*, vol. 36, no. 3, pp. 1008–1022, Mar. 2012. doi: 10.1016/j.apm.2011.07.062.

Appendix

The program Maple calculates dimensionless deflection (W bar) of plates (Al/Al_2O_3)

```
restart;
with(linalg);
pi:=evalf(Pi);
omega:=0;
t:=0;
h:=1;
m:=1;
n:=1;
a:=2*h;
Ec:=380;
```

```
Em:=70;
rhoc:=3800;
rhom:=2702;
p:=0.1;
b:=a;
qmn:=q0;
lambda:=m*pi/a;
beta:=n*pi/b;
nu:=0.3;
E(z):=Ec*exp(p*(z/h+0.5));rho(z):=rhoc*exp(p*(z/h+0.5));
C11:=E(z)/(1-nu^2);C22:=C11;C12:=nu*C11;C44:=E(z)/(2*(1+nu));
C55:=C44;C66:=C44;
f(z):=(2^5)*h*((z/((2^5)*h))-(1/3)*(z/(2*h))^3);g(z):=diff(f
(z),z);
II:=int(rho(z),z=-h/2..h/2);
I1:=evalf(int(rho(z)*z,z=-h/2..h/2));
I2:=evalf(int(rho(z)*z^2,z=-h/2..h/2));
J1:=evalf(int(rho(z)*f(z),z=-h/2..h/2));
J2:=evalf(int(rho(z)*z*f(z),z=-h/2..h/2));
K2:=evalf(int(rho(z)*(f(z))^2,z=-h/2..h/2));
A11:=int(C11,z=-h/2..h/2);
A22:=int(C22,z=-h/2..h/2);
A12:=int(C12,z=-h/2..h/2);
A66:=int(C66,z=-h/2..h/2);
B11:=int(C11*z,z=-h/2..h/2);
B22:=int(C22*z,z=-h/2..h/2);
B12:=int(C12*z,z=-h/2..h/2);
B66:=int(C66*z,z=-h/2..h/2);
D11:=int(C11*z^2,z=-h/2..h/2);
D22:=int(C22*z^2,z=-h/2..h/2);
D12:=int(C12*z^2,z=-h/2..h/2);
D66:=int(C66*z^2,z=-h/2..h/2);
Bs11:=evalf(int(C11*f(z),z=-h/2..h/2));
Bs22:=evalf(int(C22*f(z),z=-h/2..h/2));
Bs12:=evalf(int(C12*f(z),z=-h/2..h/2));
Bs66:=evalf(int(C66*f(z),z=-h/2..h/2));
Ds11:=evalf(int(C11*z*f(z),z=-h/2..h/2));
Ds22:=evalf(int(C22*z*f(z),z=-h/2..h/2));
Ds12:=evalf(int(C12*z*f(z),z=-h/2..h/2));
Ds66:=evalf(int(C66*z*f(z),z=-h/2..h/2));
Hs11:=evalf(int(C11*(f(z))^2,z=-h/2..h/2));
Hs22:=evalf(int(C22*(f(z))^2,z=-h/2..h/2));
Hs12:=evalf(int(C12*(f(z))^2,z=-h/2..h/2));
Hs66:=evalf(int(C66*(f(z))^2,z=-h/2..h/2));
```

```
As44:=evalf(int(C44*(g(z))^2,z=-h/2..h/2));
As55:=evalf(int(C55*(g(z))^2,z=-h/2..h/2));
lambda:=m*pi/a;
mu:=n*pi/b;
k11:=A11*(lambda)^2+A66*(mu)^2;
k12:=(A12+A66)*lambda*mu;
k13:=-B11*(lambda)^3-(B12+2*B66)*lambda*(mu)^2;
k14:=evalf(-Bs11*(lambda)^3-(Bs12+2*Bs66)*lambda*(mu)^2);
k22:=A66*(lambda)^2+A22*mu*(lambda)^2;
k23:=-B22*(mu)^3-(B12+2*B66)*mu*(lambda)^2;
k24:=evalf(-Bs22*(mu)^3-(Bs12+2*Bs66)*mu*(lambda)^2);
k33:=D11*(lambda)^4+2*(D12+2*D66)*(mu)^2*(lambda)^2+D22*(mu)^4;
k34:=evalf(Ds11*(lambda)^4+2*(Ds12+2*Ds66)*(mu)^2*(lambda)^2+
Ds22*(mu)^4);
k44:=Hs11*(lambda)^4+2*(Hs12+2*Hs66)*(mu)^2*(lambda)^2+Hs22*
(mu)^4+As55*(lambda)^2+As44*(mu)^2;
m11:=II;
m22:=m11;
m12:=0;
m13:=-lambda*I1;
m14:=-lambda*J1;
m23:=-mu*I1;
m24:=-mu*J1;
m33:=II+I2*((lambda)^2+(mu)^2);
m34:=J2*((lambda)^2+(mu)^2);
m44:=K2*((lambda)^2+(mu)^2);
R:=Matrix([[ k11 , k12 , k13 , k14 ],
[ k12 , k22 , k23 , k24 ],
[ k13 ,k23 ,k33 , k34 ],
[ k14, k24 , k34 , k44 ]]);
M:=Matrix([[ m11 , m12 ,m13 , m14 ],
[ m12 , m22 , m23 ,m24 ],
[m13 , m23 , m33 , m34 ],
[ m14 , m24 , m34 , m44 ]]);
X:=R-(omega)^2*M;
q:=Vector[column]([ 0 , 0 ,qmn , 0 ]);
sol:=linsolve(X,q);
umn:=sol[1];
vmn:=sol[2];
xmn:=sol[3];
ymn:=sol[4];
x:=a/2;y:=b/2;
u0:=umn*cos(lambda*x)*sin(mu*y)*exp(i*omega*t);
v0:=vmn*sin(lambda*x)*cos(mu*y)*exp(i*omega*t);
```

```
w0:=xmn*sin(lambda*x)*sin(mu*y)*exp(i*omega*t);
phi0:=ymn*sin(lambda*x)*sin(mu*y)*exp(i*omega*t);
w:=w0;
W (bar):=(10*Ec*(h)^(3)*w)/((q0*(a)^(4)));
```